IEEE Access
Multidisciplinary | Rapid Review | Open Access Journal

Received March 14, 2021, accepted April 21, 2021, date of publication May 17, 2021, date of current version May 26, 2021.

Digital Object Identifier 10.1109/ACCESS.2021.3081146

A Data-Assimilation Based Method for Equilibrium Reconstruction of Magnetic Fusion Plasma and Its Application to Reversed Field Pinch

AKIO SANPEI[1], (Member, IEEE), TAKAYUKI OKAMOTO[1], SADAO MASAMUNE[1,2], AND YASUAKI KUROE[1,3,4], (Life Member, IEEE)

[1]Department of Electronics, Kyoto Institute of Technology, Kyoto 606-8585, Japan
[2]College of Engineering, Chubu University, Kasugai 487-8501, Japan
[3]Faculty Engineering Science, Kansai University, Osaka 564-8680, Japan
[4]Organization for Research Initiatives and Development, Doshisha University, Kyoto 602-8580, Japan

Corresponding author: Akio Sanpei (sanpei@kit.ac.jp)

This work was supported in part by the Kansai Research Foundation for Technology Promotion, 2018, in part by the Kansai University Fund for the Promotion and Enhancement of Education and Research, 2018, "Development of System Analysis and Design Methods Integrating Model and Data Premised on IOT Technology," in part by the National Institute for Fusion Sciences under Grant NIFS20KOAP035 and Grant NIFS20KLEP037, and in part by the Japan Society for the Promotion of Science KAKENHI under Grant 18K11483 and Grant 20KK0063.

ABSTRACT Carbon-free energy sources are essential to avoid global warming, and nuclear fusion is expected to play a major role in achieving clean and sustainable energy. In the development of magnetic fusion, there exist a lot of issues related with plasma equilibrium to be studied extensively, typical representative of which is a problem of equilibrium reconstruction of plasma. In this paper we propose a new method of equilibrium reconstruction for fusion plasma based on the data assimilation. Aiming at dealing not only with axisymmetric toroidal plasmas but also with more general toroidal plasmas, we formulate the problems of equilibrium reconstruction in generalized forms and derive methods to solve them. We also propose a method for applying the equilibrium reconstruction method to the reversed field pinch (RFP), and it is applied to a real RFP experimental apparatus for its evaluation. It is shown through numerical experiments that the proposed equilibrium reconstruction method works well with reasonable accuracy. And it is also shown through real experiments applying the RFP apparatus that the equilibrium of RFP plasma is appropriately reconstructed.

INDEX TERMS Data assimilation, equilibrium reconstruction, fusion plasma, inverse problems, sensitivity equation.

I. INTRODUCTION

Development of carbon-free energy sources with a less load to the environment is one of the urgent issues in ensuring human society and maintaining the sustainability of development. Nuclear fusion is one of the candidates for the solution, and development of fusion reactor has been in progress to realize electric energy production from virtually unlimited fuel sources [1], [2]. The International Thermonuclear Experimental Reactor, dubbed ITER, is under construction in France in the framework of international collaboration among major countries and organizations over the world [3]. The initial operation for plasma production in ITER is scheduled in 2025.

In order to realize fusion plasma, the plasma has to be maintained in an equilibrium state where electromagnetic force acting on a plasma element balances with pressure force. There exist a lot of issues related with plasma equilibrium to be studied extensively, typical representative of which is a problem of equilibrium reconstruction of plasma. The objective of this paper is to propose a new method for reconstructing the equilibrium state of magnetic fusion plasma and to propose a method for applying it to reversed field pinch (RFP). Some research programs for the RFP configuration

The associate editor coordinating the review of this manuscript and approving it for publication was Paolo Bettini.

are in progress because of its potential of a compact fusion reactor [4]–[8].

Rigorous (accurate) modeling and mathematical formulation of the equilibrium for fusion plasma are difficult problems. In spite of the difficulties, many efforts have been made to develop their mathematical models and some nonlinear partial differential equations which are appropriate to describe the equilibrium are derived; the derived partial differential equations contain unknown parts. The equilibrium reconstruction is an inverse problem to obtain solutions of the partial differential equations with identifying the unknown parts, which can appropriately reproduce experimental data. There have been several studies done on the problem of equilibrium reconstruction for axisymmetric toroidal plasmas [9]–[15]. A brief historical description of the studies is given in the next section (II. RELATED WORKS).

In this paper we propose a new method of equilibrium reconstruction for fusion plasma based on the data assimilation. In the last decades, data assimilation has attracted much attention especially in simulations and estimations of large scale complex systems with less rigorous modeling. There have been several methods and algorithms developed, and a lot of efforts have been made for applying them to solving inverse problems in various fields from environmental sciences, atmospheric sciences, geosciences, biology to human and social sciences [16]–[20]. In equilibrium reconstruction of fusion plasma, it often happens that we do not have enough information for characterizing the equilibrium. Under these circumstances, we have to make use of as much experimental data as possible for equilibrium reconstruction, which implies that the introduction of the data assimilation is very promising.

Aiming at applying not only to axisymmetric toroidal plasmas but also to more general toroidal plasmas, we formulate the problems of equilibrium reconstruction in generalized forms and derive methods to solve them. The mathematical model of equilibrium states for axisymmetric toroidal plasma is reduced to a single partial differential equation, known as the Grad-Shafranov (GS) equation [21], [22]. In a plasma without toroidal symmetry, if magnetic surfaces exist, the equilibrium is described by three partial differential equations for three scalar functions [23]. In the present stage of mathematical modeling of equilibrium states, no model consisting of more than three partial differential equations has been proposed. In our problem formulation, however, we consider, as the target equations, a model consisting of more than three partial differential equations taking account of the possibility of future development of some extended mathematical model of equilibrium states.

The reconstruction problem is formulated as follows. We parameterize the uncertainties and unknowns in the target equations by introducing adjustable parameters. A cost function is defined as the errors between experimental measurement data and the corresponding ones obtained from the solutions of the target equations. The reconstruction is formulated as an optimization problem to determine a set of unknown adjustable parameters which minimizes the cost function.

Optimization problem of this kind is usually solved by use of the gradient method such as the steepest descent method, the conjugate gradient method, the quasi-Newton method and so on, and the same is true for data assimilation. It should be noted that calculation of the gradient vector of the cost function with respect to the unknown parameters remains one of the issues to be studied carefully. In the present work, a set of the sensitivity equations is derived. By parametrization of the target equations, there appears a specific point where the solution or its gradient takes a specified value. In deriving the sensitivity equations we have paid special attention to take it into account appropriately. Furthermore, we explain how to solve the target equations and their sensitivity equations with emphasizing how to deal with the specific point.

We also propose a method for applying the proposed equilibrium reconstruction method to the RFP. In developing the method we use the RFP experimental apparatus REversed Field Pinch of Low Aspect ratio eXperiment (RELAX) [24] developed at Kyoto Institute of Technology. We have performed numerical experiments in order to evaluate accuracy of the proposed method and real experiments by using RELAX. In deriving sensitivity equations we have paid special attention to take account of the specific point (location of the magnetic axis) as a boundary condition. It is shown through numerical experiments that the equilibrium of the plasma is reconstructed with reasonable accuracy. It is also shown through real experiments that the proposed method works well for real data and the equilibrium of RELAX is appropriately reconstructed.

II. RELATED WORKS

In toroidal plasmas, the poloidal magnetic field plays the role of maintaining the equilibrium and the toroidal magnetic field plays the role of stabilization. There are two magnetic confinement configurations in axisymmetric toroidal plasmas; one is the tokamak, and the other is the RFP. In the tokamak the toroidal magnetic field is much stronger than the poloidal field, and the equilibrium is described by the GS equation under the assumption of the existence of magnetic flux surfaces, which assumption is appropriate under strong toroidal field. Many works have been done on the equilibrium reconstruction problems based on the GS equation [9]–[14], [25]–[27].

In early phase of tokamak researches, equilibrium reconstruction was performed in order to compare theoretical (or model) magnetic field profiles with those obtained from experimental data for detailed studies of equilibrium and its stability [25]. In such cases, the unknown parts of the GS equation were represented in various functional forms of the poloidal flux function; exponential approximation of the radial profiles was one of the examples [13]. For the purpose of improving the efficiency in equilibrium studies, efforts have been devoted to reducing computation time with keeping sufficient accuracy of the reconstruction results by

developing appropriate modeling (parametrization, or, functional forms) of the unknown parts of the GS equation and by developing adequate methods for solving the GS equation and for solving the optimization problem [9]. Moreover, as the capability of computers advances, real time control of the plasma shape or plasma position has been required in order to improve plasma performance, the need for associated real time equilibrium reconstruction has also been increased. In the modeling of the unknown parts of the GS equation, a representative form of the unknown parts is such that unknown parameters are assigned to the coefficients of polynomials of the flux function [9], [13]. This choice of parametrization of the unknown parts has the advantage that with the use of Picard iteration scheme [28] the solution to the GS equation can be expressed as a product of a vector whose components are the unknown parameters and a response matrix. The solution of the optimization problem for the equilibrium reconstruction can be obtained by solving a matrix equation, for example, by the use of the singular value decomposition (SVD) method, which reduces computational time drastically [10], [12]–[14], and equilibrium reconstruction has become used for real-time plasma control [11], [27]. More recently similar parametrization is widely used in equilibrium reconstruction for detailed studies of equilibrium and for real time control of the tokamak plasma [26].

In contrast to the tokamak, magnitude of the toroidal magnetic field is comparable to that of the poloidal magnetic field in the RFP, which allows growth of magnetohydrodynamic (MHD) instabilities. The traditional concept of the RFP equilibrium has been that the RFP configuration is a result of MHD relaxation (relaxation to a near-minimum energy state), and is sustained by the help of nonlinearly interacting MHD instabilities. Magnetic surfaces exist in the average sense, where the magnetic field lines are averaged over the time period longer than the growth time of the MHD instabilities in the time domain and over the scale lengths longer than the characteristic wavelengths of the instabilities in the spatial domain. The basic model for the relaxed state is the force-free equilibrium [29], which has been advanced by taking account of the boundary conditions and by including the effects of perpendicular (diamagnetic) current [30]. Thus, few studies have been done on the equilibrium reconstruction of RFP plasmas based on the GS equation. The traditional concept of the RFP equilibrium has been changed by the successes of realizing the improved confinement states brought about by the inductive current profile control [31], or by either spontaneous or controlled transition (relaxation) to the helically deformed RFP states [32], [33], where suppression of the MHD instabilities has led to the recovery of instantaneous magnetic surfaces. In particular, motivated by the success of the inductive current profile control [31], the first work on the equilibrium reconstruction based on the GS equation was done in [15], which is the only major publication about axisymmetric RFP equilibrium reconstruction to date. Further progress in the RFP research can be found in a recent review of the RFP [34].

In the equilibrium reconstruction based on the GS equation, one of the important problems is how to approximate its unknown parts. The polynomial model is powerful in reducing computation time for tokamak plasmas as described above, it does not provide a good approximation to describe RFP equilibrium which is based on the MHD relaxed states [35]. In [15], a method is proposed of RFP equilibrium reconstruction, in which the unknown parts of the GS equation are approximated by using spline interpolation through several points including unknown parameters. In their method, the equilibrium equation can no longer be represented as a linear matrix equation, and therefore determination of the parameters is reduced to solving a nonlinear optimization problem. They solve the nonlinear optimization problem by the amoeba method [36] which does not require calculation of gradients of the cost function. There remain some problems to be solved in improving the reconstruction method for the RFP plasma such as modeling of the unknown parts (of the GS equation) and improvement of the method for solving the nonlinear optimization problem.

III. PROBLEM FORMULATION OF EQUILIBRIUM RECONSTRUCTION AS DATA ASSIMILATION

In this section we formulate equilibrium reconstruction problem for magnetic fusion plasma as a data assimilation. Aiming at dealing not only with axisymmetric toroidal plasmas but also with non-axisymmetric toroidal plasmas and to plasmas described by some future perspective model, we formulate the problems of equilibrium reconstruction in generalized forms. We consider a system described by the following partial differential equation in the three dimensional space $\boldsymbol{R}^3$.

$$\mathcal{L}_k \psi_k(\boldsymbol{x}) = f_k^o(\boldsymbol{x}, \psi_1(\boldsymbol{x}), \psi_2(\boldsymbol{x}), \cdots, \psi_K(\boldsymbol{x})), \quad \boldsymbol{x} \in \boldsymbol{D} \subset \boldsymbol{R}^3, \quad k = 1, 2, \cdots, K \tag{1}$$

where $\psi_k \in \boldsymbol{R}$ is the scalar quantity characterizing the equilibrium state of the fusion plasma, $\mathcal{L}_k$ is a partial differential operator with respect to the spatial variable $\boldsymbol{x}$ including high order partial derivatives. $\boldsymbol{D}\left(\subset \boldsymbol{R}^3\right)$ is an open region in which the scalar function $\psi_k(\boldsymbol{x})$ is defined. f_k^o is a nonlinear function ($f_k^o : \boldsymbol{R}^3 \times \underbrace{\boldsymbol{R} \times \cdots \times \boldsymbol{R}}_{K} \to \boldsymbol{R}$). For an axisymmetric toroidal plasma such as standard tokamak or RFP, the equilibrium is described by a single partial differential equation ($K = 1$), the partial differential operator $\mathcal{L}_1$ is known as the Grad-Shafranov operator and equation (1) is known as the GS equation. For a plasma, if the magnetic surfaces exist, the plasma equilibrium can be described by a set of nonlinear partial differential equations with respect to three scalar functions ($K = 3$) [23]. In the above formulation, we consider a model consisting of more than three partial differential equations taking account of the possibility of future development of some prospective model of equilibrium states ($K > 3$).

The boundary condition of the partial differential equation (1) is given as follows.

$$f_k^{Bo}(\psi_1(\boldsymbol{x}), \psi_2(\boldsymbol{x}), \cdots, \psi_K(\boldsymbol{x}), \mathcal{L}_1^B\psi_1(\boldsymbol{x}), \mathcal{L}_2^B\psi_2(\boldsymbol{x}), \cdots, \mathcal{L}_K^B\psi_K(\boldsymbol{x})) = 0, \quad \boldsymbol{x} \in \partial\boldsymbol{D}, \quad k = 1, 2, \cdots, K \tag{2}$$

where $\partial\boldsymbol{D}$ is the boundary of the region $\boldsymbol{D}$ and f_k^{Bo} is a nonlinear function ($f_k^{Bo} : \underbrace{R \times \cdots \times R}_{2K} \to R$). The operator $\mathcal{L}_k^B$ is the differential operator whose order is lower than that of $\mathcal{L}_k$.

The equilibrium reconstruction problem is to obtain the solution of the partial differential equation (1) with the boundary condition (2) for given functions f_k^o and f_k^{Bo}. However it is almost impossible to give these functions exactly in actual magnetic fusion plasma. We introduce the concept of data assimilation to the equilibrium reconstruction problem. By using the information obtained from several sensors attached to the plasma device, the problem is formulated as follows. Introducing an adjustable vector parameter, we parameterize uncertainties and unknowns in f_k^o and f_k^{Bo}. Let $\boldsymbol{p} = [p_1, \cdots, p_{N_p}]^t$ be the adjustable vector parameter whose number of elements is N_p. We call $p_i (i = 1, \cdots, N_p)$ the free parameters. By the parametrization, (1) and (2) become:

$$\mathcal{L}_k\psi_k(\boldsymbol{x}) = f_k(\boldsymbol{x}, \psi_1(\boldsymbol{x}), \psi_2(\boldsymbol{x}), \cdots, \psi_K(\boldsymbol{x}), \psi_1(\boldsymbol{x}_{ex}), \psi_2(\boldsymbol{x}_{ex}), \cdots, \psi_K(\boldsymbol{x}_{ex}), \boldsymbol{p}), \quad \boldsymbol{x} \in \boldsymbol{D} \subset \boldsymbol{R}^3, \quad k = 1, 2, \cdots, K \tag{3}$$

where $\boldsymbol{x}_{ex}$ is a point where the gradient of ψ_k takes a known value $\boldsymbol{c}$ as follows,

$$\frac{\partial\psi_k}{\partial\boldsymbol{x}}(\boldsymbol{x}_{\mathrm{ex}}) = \boldsymbol{c}_k, \quad k = 1, 2, \cdots, K, \tag{4}$$

and

$$f_k^B(\psi_1(\boldsymbol{x}), \psi_2(\boldsymbol{x}), \cdots, \psi_K(\boldsymbol{x}), \mathcal{L}_1^B\psi_1(\boldsymbol{x}), \mathcal{L}_2^B\psi_2(\boldsymbol{x}), \cdots, \mathcal{L}_K^B\psi_K(\boldsymbol{x}), \boldsymbol{p}) = 0, \quad \boldsymbol{x} \in \partial\boldsymbol{D}, \quad k = 1, 2, \cdots, K. \tag{5}$$

The condition (4) appears by parametrization of the target equation. For example, $\boldsymbol{x}_{ex}$ is a point where $\psi_k(\boldsymbol{x})$ takes an extremum in the region $\boldsymbol{D}$ if $\boldsymbol{c}_k = \boldsymbol{0}$. In parameterizations, in general, the scalar quantity $\psi_k(\boldsymbol{x})$ is often normalized by its maximum or minimum value, which brings the condition (4). The equilibrium reconstruction problem based on data assimilation in this paper is to solve the partial differential equations (3) and (4) under the boundary condition (5) and to obtain the free parameter $\boldsymbol{p}$ simultaneously.

The free parameter $\boldsymbol{p}$ will be determined by using the data obtained from sensors as follows. Let N_m be the number of sensors attached to the plasma device and d_i, the data from the i-th sensor ($i = 1, 2, \cdots, N_m$). Suppose that the sensing process of the i-th sensor is modeled mathematically by the following equation

$$m_i = f_{m_i}(\psi_1(\boldsymbol{x}), \psi_2(\boldsymbol{x}), \cdots, \psi_K(\boldsymbol{x}), \mathcal{L}_1^{m_i}\psi_1(\boldsymbol{x}), \mathcal{L}_2^{m_i}\psi_2(\boldsymbol{x}), \cdots, \mathcal{L}_K^{m_i}\psi_K(\boldsymbol{x}), \boldsymbol{p}), \quad i = 1, 2, \cdots, N_m \tag{6}$$

where f_{m_i} is a mapping from $\underbrace{L(\boldsymbol{D}) \times \cdots \times L(\boldsymbol{D})}_{2K} \times N_p$ to $\boldsymbol{R}$, and $L(\boldsymbol{D})$ is an appropriate function space defined in the region $\boldsymbol{D}$, and m_i is the output of the i-th sensing process. The operator $\mathcal{L}_k^{m_i}$ is the differential operator whose order is lower than that of $\mathcal{L}_k$. For example, f_{m_i} is a weighted integral equation over the sensing area. If the weighting function is the delta function, f_{m_i} corresponds to one point measurement process. The problem is now to determine the parameter $\boldsymbol{p}$ such that the real data d_i become equal to the outputs m_i of the mathematical model (6). We define the following cost function

$$E(\boldsymbol{p}) = \frac{1}{2}\sum_{i=1}^{N_m} w_i e_i^2 = \frac{1}{2}\sum_{i=1}^{N_m} w_i (m_i - d_i)^2 \tag{7}$$

where $w_i \geq 0$ is a weighting coefficient. The problem of data assimilation becomes a problem of finding the parameter $\boldsymbol{p}$ which minimizes the cost function (7) under the constraints (3), (4), (5) and (6). It is formulated as the following optimization problem with equality constraints.

$$\begin{aligned} &\underset{\boldsymbol{p}}{\text{minimize}}\ E(\boldsymbol{p}) \\ &\text{subject to (3), (4), (5) and (6)} \end{aligned} \tag{8}$$

If we can solve the above optimization problem, the solution of (3), (4) and (5) for the optimal parameter $\boldsymbol{p}^*$ is the equilibrium state of the target plasma consistent with experimental data.

IV. PROPOSED METHOD

A. METHOD OF EQUILIBRIUM ESTIMATION BASED ON DATA ASSIMILATION

The constrained optimization problem (8) can be solved by using a gradient based method such as the steepest descent method, conjugate gradient method, quasi-Newton method and so on. In these algorithms, the gradient of the cost function (7) with respect to $\boldsymbol{p}$ has to be calculated. In order to obtain the gradient, two methods are conceivable; one is a method of deriving the sensitivity equations and the other deriving the adjoint equation. In this paper, the sensitivity equations are derived. In deriving the sensitivity equations the fact that the parametrized mathematical model (3) of the target plasma depends on the point $\boldsymbol{x}_{ex}$ satisfying (4) should be considered. In the following we discuss a method to derive the sensitivity equations.

Differentiating (7) with respect to the j-th element of $\boldsymbol{p}$, denoted by p_j, we obtain:

$$\frac{\partial E}{\partial p_j} = \sum_{i=1}^{N_m} w_i e_i \frac{\partial e_i}{\partial p_j} = \sum_{i=1}^{N_m} w_i e_i \frac{\partial m_i}{\partial p_j}. \tag{9}$$

For calculating $\partial m_i/\partial p_j$, we derive the sensitivity equations for the partial differential equations (3) and (4) under the boundary condition (5) together with the mathematical model of the sensing process (6). In the following, we will derive the sensitivity equations for the case $k = 1$, those for the case $k > 1$ can be obtained in the similar manner. In order to simplify the mathematical expression in the derivation, the suffix $k(= 1)$ is omitted and the arguments of f, f^B and f_m are represented by $\boldsymbol{x}$, ψ and $\boldsymbol{p}$, where ψ stands for ψ_k and their spatial derivatives $\mathcal{L}_k^B\psi_k$ and $\mathcal{L}_k^{m_i}\psi_k$ $(k = 1)$. Then, (3), (4), (5), (6) are expressed as follows:

$$\mathcal{L}\psi(\boldsymbol{x},\boldsymbol{p}) = f(\boldsymbol{x}, \psi(\boldsymbol{x},\boldsymbol{p}), \psi(\boldsymbol{x}_{\rm ex}(\boldsymbol{p}),\boldsymbol{p}),\boldsymbol{p}), \quad \boldsymbol{x} \in \boldsymbol{D} \subset \boldsymbol{R}^3. \tag{10}$$

$$\frac{\partial\psi}{\partial\boldsymbol{x}}(\boldsymbol{x}_{\rm ex}(\boldsymbol{p}),\boldsymbol{p}) = \boldsymbol{c}_{\rm ex}. \tag{11}$$

$$f^B(\psi(\boldsymbol{x}),\boldsymbol{p}) = 0, \quad \boldsymbol{x} \in \partial\boldsymbol{D}. \tag{12}$$

$$m_i = f_{m_i}(\psi(\boldsymbol{x}),\boldsymbol{p}), \quad i = 1, 2, \cdots, N_m. \tag{13}$$

It should be noted that the point $\boldsymbol{x}_{ex}$ depends on the parameter $\boldsymbol{p}$. Differentiating both sides of (10) with respect to p_j, we obtain the following equation:

$$\mathcal{L}\frac{\partial\psi}{\partial p_j} = \frac{\partial f}{\partial\psi}\frac{\partial\psi}{\partial p_j} + \frac{\partial f}{\partial\psi(\boldsymbol{x}_{ex})}\left(\frac{\partial\psi(\boldsymbol{x}_{ex})}{\partial p_j} + \frac{\partial\psi(\boldsymbol{x}_{ex})}{\partial\boldsymbol{x}}\frac{\partial\boldsymbol{x}_{ex}}{\partial p_j}\right) + \frac{\partial f}{\partial p_j}, \quad \boldsymbol{x} \in \boldsymbol{D} \subset \boldsymbol{R}^3. \tag{14}$$

Differentiation of both sides of the boundary condition (12) gives

$$\frac{\partial f^B}{\partial\psi}\frac{\partial\psi}{\partial p_j} + \frac{\partial f^B}{\partial p_j} = 0, \quad \boldsymbol{x} \in \partial\boldsymbol{D}. \tag{15}$$

Equation (14) is a partial differential equation with respect to the sensitivity $\partial\psi/\partial p_j$ being unknown variables, and (15) is its boundary condition. Therefore, the gradient $\partial E/\partial\boldsymbol{p}$ is obtained by solving (14) and (15) for all j $(j = 1, 2, \cdots, N_p)$. All the terms in (14) and (15) except $\partial\boldsymbol{x}_{ex}/\partial p_j$ can be obtained from the solution of the original partial differential equation (10), (11) and its boundary condition (12).

$\partial\boldsymbol{x}_{ex}/\partial p_j$ is calculated as follows. Differentiating both sides of (11) and arranging the result, we obtain:

$$\frac{\partial\boldsymbol{x}_{ex}}{\partial p_j} = -\frac{\partial^2\psi(\boldsymbol{x}_{ex})}{\partial\boldsymbol{x}^2}^{-1}\frac{\partial}{\partial\boldsymbol{x}}\frac{\partial\psi(\boldsymbol{x}_{ex})}{\partial p_j}. \tag{16}$$

Substituting (16) into (14), the following equation is obtained,

$$\mathcal{L}\frac{\partial\psi}{\partial p_j} = \frac{\partial f}{\partial\psi}\frac{\partial\psi}{\partial p_j} + \frac{\partial f}{\partial\psi(\boldsymbol{x}_{ex})}\left(\frac{\partial\psi(\boldsymbol{x}_{ex})}{\partial p_j} - \frac{\partial\psi(\boldsymbol{x}_{ex})}{\partial\boldsymbol{x}}\frac{\partial^2\psi(\boldsymbol{x}_{ex})}{\partial\boldsymbol{x}^2}^{-1}\frac{\partial}{\partial\boldsymbol{x}}\frac{\partial\psi(\boldsymbol{x}_{ex})}{\partial p_j}\right) + \frac{\partial f}{\partial p_j}, \quad \boldsymbol{x} \in \boldsymbol{D} \subset \boldsymbol{R}^3. \tag{17}$$

Equation (17) is now the partial differential equation with respect to $\partial\psi/\partial p_j$ being unknown variables, in which all the terms are obtained from the solution of (10), (11) and (12). Note that $\boldsymbol{x}_{ex}$ is obtained by finding a point which satisfies (11) for the solution. Equation (17) under the boundary condition (15) provides the sensitivity $\partial\psi/\partial p_j$, and it is called the sensitivity equation. The gradient $\partial E/\partial\boldsymbol{p}$ is calculated by using the sensitivity $\partial\psi/\partial p_j$ as follows.

The differentiation of (13) with respect to p_j leads to the following equation,

$$\frac{\partial m_i}{\partial p_j} = \frac{\partial f_{m_i}}{\partial\psi}\frac{\partial\psi}{\partial p_j} + \frac{\partial f_{m_i}}{\partial p_j}, \quad i = 1, 2, \cdots, N_m. \tag{18}$$

Since $\partial f_{m_i}/\partial\psi$ and $\partial f_{m_i}/\partial p_j$ in the right hand side of (18) are calculated by using the solution ψ of (10), (11) and (12), $\partial m_i/\partial p_j$ is calculated by using the sensitivity $\partial\psi/\partial p_j$ and the solution ψ. The gradient of the cost function can be calculated from (9).

The optimization problem (8) can be solved by using the gradient $\partial E/\partial\boldsymbol{p}$ thus obtained. Its procedure is summarized as the following algorithm.

[Algorithm for Equilibrium Reconstruction]

Step1 Set an initial guess $\boldsymbol{p}^0$ for the free parameter $\boldsymbol{p}$.

Step2 Solve the partial differential equation (10), (11) and (12). Obtain m_i by calculating (13).

Step3 Solve the sensitivity equations (17) under the boundary conditions (15) for $j = 1, 2, \cdots, N_p$. Obtain $\partial m_i/\partial p_j$ by calculating (18) for $i = 1, 2, \cdots, N_m$ and $j = 1, 2, \cdots, N_p$.

Step4 Obtain the gradient $\partial E/\partial\boldsymbol{p}$ by calculating (7) and (9), and by using the results of Steps 2 and 3.

Step5 If $|\partial E/\partial\boldsymbol{p}|$ is small enough, stop. If not, update $\boldsymbol{p}^{(k_o)}$ to $\boldsymbol{p}^{(k_o+1)}$ according to an appropriate gradient based method such as the steepest descent method, conjugate gradient method, quasi-Newton method, and go to Step 2. The superscript k_o is the iteration number for optimization.

The algorithm for $k > 1$ can be described in the same form.

B. METHOD FOR SOLVING THE TARGET EQUATION AND ITS SENSITIVITY EQUATIONS

In this section, we describe how to solve the partial differential equation (10) with (11) and (12) in Step 2 for the target plasma and its sensitivity equations (17) and (15) in Step 3.

Since the partial differential equation (10) with (11) and (12) is nonlinear, we use the Green's function method and Picard's iteration method [28]. Note that in solving them it is necessary to find the point $\boldsymbol{x}_{\rm ex}$ which satisfies (11). The Green's function is defined as the solution of the following equation

$$\mathcal{L}G(\boldsymbol{x}) = \delta(\boldsymbol{x} - \boldsymbol{x}') \tag{19}$$

with the boundary condition (12), and denoted by $G(\boldsymbol{x}';\boldsymbol{x})$. Using the Green's function, the original partial differential equation is transformed to the following integral equation.

$$\psi(\boldsymbol{x}) = \int_{\boldsymbol{D}} G(\boldsymbol{x}';\boldsymbol{x}) f(\boldsymbol{x}', \psi(\boldsymbol{x}'), \psi(\boldsymbol{x}_{ex}), \boldsymbol{p}) d\boldsymbol{x}'. \tag{20}$$

In the above equation, $\psi(\boldsymbol{x_{ex}})$ should be expressed using the delta function as follows

$$\psi(\boldsymbol{x}) = \int_{\boldsymbol{D}} G(\boldsymbol{x'}; \boldsymbol{x}) f(\boldsymbol{x'}, \psi(\boldsymbol{x'}), \psi(\boldsymbol{x'}) \times \delta(\boldsymbol{x'} - \boldsymbol{x_{ex}}), \boldsymbol{p}) d\boldsymbol{x'}. \tag{21}$$

Discretizing the region $\boldsymbol{D}$ into grid points, the number of which is denoted by N and i-th grid point by x_i, the above integral equation becomes the following equation

$$\vec{\psi} = \mathbb{G} \cdot \boldsymbol{f}(\vec{\psi}, \psi(x_{ex})). \tag{22}$$

For simplicity, we assume that the point $\boldsymbol{x}_{ex}$ is equal to one of the grid points, which is denoted by x_{ex}. In (22), $\vec{\psi}$ is the N dimensional vector whose i-th element is $\psi(x_i)$, $\mathbb{G}$ is the $N \times N$ matrix whose (i, j)-th element is $G(x_j; x_i)$, and $\boldsymbol{f}$ is the N dimensional vector whose j-th element is $f(x_j, \vec{\psi}(x_j), \psi(x_{ex}), \boldsymbol{p})$. Because $\boldsymbol{f}$ is a nonlinear function of $\vec{\psi}$, in order to solve (22) it is necessary to use an appropriate iterative method. We use the Picard's iteration method [28] which gives the following recurrence formula:

$$\vec{\psi}^{k_P+1} = \mathbb{G} \cdot \boldsymbol{f}(\vec{\psi}^{k_P}, \psi(x_{ex})^{k_P}) \tag{23}$$

where the superscript k_P is the iteration number. Note that, since $\boldsymbol{f}$ is a function of the point x_{ex}, at each iteration it is necessary to find x_{ex} from $\vec{\psi}^{k_P}$ by using the condition (11) in order to calculate the right hand side of (23).

Next, we explain how to solve the sensitivity equations (17) under (15). Similar to (21) of the original partial differential equation, the solution of the sensitivity equations can be expressed by using the same Green's function defined by (19) as follows

$$\frac{\partial \psi(\boldsymbol{x})}{\partial p_j} = \int_{\boldsymbol{D}} G(\boldsymbol{x'}; \boldsymbol{x}) \times h\left(\boldsymbol{x'}, \frac{\partial \psi(\boldsymbol{x'})}{\partial p_j}, \frac{\partial \psi(\boldsymbol{x_{ex}})}{\partial p_j}, \frac{\partial}{\partial \boldsymbol{x'}} \frac{\partial \psi(\boldsymbol{x_{ex}})}{\partial p_j}, \boldsymbol{p}\right) d\boldsymbol{x'} \tag{24}$$

where h comes from the right hand side of the sensitivity equation (17), and is described by

$$\begin{aligned} &h\left(\boldsymbol{x}, \frac{\partial \psi(\boldsymbol{x})}{\partial p_j}, \frac{\partial \psi(\boldsymbol{x_{ex}})}{\partial p_j}, \frac{\partial}{\partial \boldsymbol{x}} \frac{\partial \psi(\boldsymbol{x_{ex}})}{\partial p_j}, \boldsymbol{p}\right) \\ &= \frac{\partial f}{\partial \psi} \frac{\partial \psi}{\partial p_j} + \frac{\partial f}{\partial \psi(\boldsymbol{x_{ex}})} \left(\frac{\partial \psi(\boldsymbol{x})}{\partial p_j} \right. \\ &\quad \left. - \frac{\partial \psi(\boldsymbol{x_{ex}})}{\partial \boldsymbol{x}} \frac{\partial^2 \psi(\boldsymbol{x_{ex}})}{\partial \boldsymbol{x}^2}^{-1} \frac{\partial}{\partial \boldsymbol{x}} \frac{\partial \psi(\boldsymbol{x})}{\partial p_j} \right) \\ &\quad \times \delta(\boldsymbol{x} - \boldsymbol{x_{ex}}) + \frac{\partial f}{\partial p_j}. \end{aligned} \tag{25}$$

Note that, similar to (21), the second and third terms including $\boldsymbol{x}_{ex}$ in h should be expressed using the delta function. As a result, the right hand side of (24) is calculated as follows

$$\begin{aligned} \frac{\partial \psi(\boldsymbol{x})}{\partial p_j} &= \int_{\boldsymbol{D}} G(\boldsymbol{x'}; \boldsymbol{x}) \left(\frac{\partial f}{\partial \psi} \frac{\partial \psi}{\partial p_j} + \frac{\partial f}{\partial p_j} \right) d\boldsymbol{x'} \\ &\quad + G(\boldsymbol{x_{ex}}; \boldsymbol{x}) \frac{\partial}{\partial \psi(\boldsymbol{x}_{ex})} f(\boldsymbol{x}_{ex}, \psi(\boldsymbol{x}_{ex}), \psi(\boldsymbol{x}_{ex}), p) \\ &\quad \times \left(\frac{\partial \psi(\boldsymbol{x}_{ex})}{\partial p_j} - \frac{\partial \psi(\boldsymbol{x}_{ex})}{\partial \boldsymbol{x}} \frac{\partial^2 \psi(\boldsymbol{x}_{ex})}{\partial \boldsymbol{x}^2}^{-1} \frac{\partial}{\partial \boldsymbol{x}} \frac{\partial \psi(\boldsymbol{x}_{ex})}{\partial p_j} \right). \end{aligned} \tag{26}$$

Discretizing the region $\boldsymbol{D}$ into grid points, the above integral equation becomes the following matrix equation.

$$\vec{\psi}_j^s = \mathbb{G}\mathrm{diag}\left(\frac{\partial f(x_i)}{\partial \psi} \right) \vec{\psi}_j^s + \mathbb{G}\vec{f}_j^s + \mathbb{G}\mathbb{F}_{ex}(\vec{\psi}_j^s - \mathbb{H}\vec{\psi}_j^s) \tag{27}$$

where

$$\vec{\psi}_j^s(\boldsymbol{x}) = [\psi_j^s(x_1), \psi_j^s(x_2), \cdots, \psi_j^s(x_N)]^t := \frac{\partial \vec{\psi}(\boldsymbol{x})}{\partial p_j}, \tag{28}$$

$$\vec{f}_j^s := \frac{\partial \boldsymbol{f}}{\partial p_j} \tag{29}$$

and $\mathrm{diag}\,(\partial f(x_i)/\partial \psi)$ is the $N \times N$ matrix whose diagonal i-th element is $\partial f(x_i)/\partial \psi$. $\mathbb{F}_{ex}$ is the $N \times N$ matrix where the (ex, ex)-th element equals $\partial f(x_{ex})/\partial \psi(x_{ex})$ and all other array elements are equal to 0, i.e.,

$$\mathbb{F}_{ex} = \begin{pmatrix} 0 & \cdots & & 0 & \cdots & & 0 \\ \vdots & \ddots & & \vdots & \ddots & & \vdots \\ & & 0 & 0 & & & \\ 0 & \cdots & 0 & \dfrac{\partial f(x_{ex})}{\partial \psi(x_{ex})} & 0 & \cdots & 0 \\ \vdots & \ddots & & 0 & 0 & & \vdots \\ & & & \vdots & & \ddots & \\ 0 & \cdots & & 0 & \cdots & & 0 \end{pmatrix}. \tag{30}$$

The last term of (27) comes from the last term of (26). Noting that by a difference approximation of the differentiation $\partial/\partial \boldsymbol{x}$ of the term $(\partial/\partial \boldsymbol{x})(\partial \psi(\boldsymbol{x}_{ex})/\partial p_j)$, it is expressed as $\mathbb{H}\vec{\psi}_j^s$ with appropriately defining the matrix $\mathbb{H}$. Equation (27) can be arranged as follows,

$$\mathbb{A}_j \vec{\psi}_j^s = \mathbb{B}_j, \quad j = 1, 2, \cdots, N_p \tag{31}$$

where $\mathbb{A}_j = \mathbb{E} - \mathbb{G}\mathrm{diag}\left(\frac{\partial f(x_i)}{\partial \psi}\right) - \mathbb{G}\mathbb{F}_{ex}(\mathbb{E} - \mathbb{H})$, $\mathbb{B}_j = \mathbb{G}\vec{f}_j^s$ and $\mathbb{E}$ is the identity matrix of $N \times N$. The matrix equation (31) can be solved by using some numerical methods such as the Gauss-Seidel method, and so on. This procedure is repeated N_p times, which gives us gradient of all the parameters $\partial E/\partial \boldsymbol{p}$.

V. APPLICATION TO THE REVERSED FIELD PINCH PLASMA

In this section, we propose a method for applying to the RFP the equilibrium reconstruction method developed in the

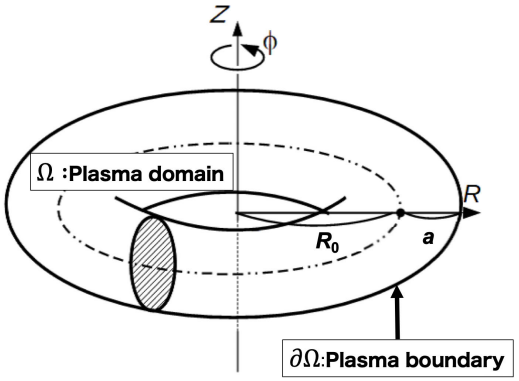

FIGURE 1. Toroidal plasma and the cylindrical coordinate system.

previous Section. We apply it to artificial numerical data generated by simulations in order to evaluate its accuracy and convergence performance. Then, it is applied to real RFP experimental data in order to evaluate its validity. The target plasma is the RFP generated in REversed Field Pinch of Low Aspect ratio eXperiment (RELAX) device [24] developed at Kyoto Institute of Technology.

In Secs.V-A and V-B, the mathematical model and parametrization of general RFP will be described. From Sec.V-C, we will concentrate our argument on RELAX plasma.

A. MATHEMATICAL MODEL OF TARGET PLASMA

Figure 1 shows the schematic drawing of a toroidal plasma and its cylindrical coordinate system (R, ϕ, Z). Let R_0 (major radius) be the distance from the Z axis to the geometric center of the torus small circle and the radius of the small circle be a (minor radius, same as the radius of the plasma). The plasma is confined by a magnetic field B_ϕ (toroidal magnetic field) in the ϕ direction and a magnetic field B_p (poloidal magnetic field) in the (R, Z) plane. B_ϕ is applied externally and also produced by the internal poloidal plasma current, while B_p is formed by the toroidal plasma current I_ϕ, the current density of which is denoted by J_ϕ.

In axisymmetric toroidal plasmas, the model (10) describing the equilibrium is represented as follows [21], [22].

$$\begin{aligned} \Delta^*\psi(R,Z) &= -\mu_0 R J_\phi(\psi(R,Z),R,Z), \\ J_\phi(\psi(R,Z),R,Z) &= \frac{2\pi F(\psi(R,Z))F'(\psi(R,Z))}{\mu_0 R} \\ &\quad + 2\pi R P'(\psi(R,Z)), \quad (R,Z)\in\Omega \end{aligned} \tag{32}$$

where Ω is the plasma domain corresponding to the whole area in the vacuum vessel, as described previously. ψ is the poloidal magnetic flux which characterizes the behavior of the confined plasma. F is the poloidal current function $F(\psi(R,Z)) = RB_\phi(R,Z)$ and P is the pressure function. In the above equation, $F'$and P' are $F' = dF/d\psi$ and $P' = dP/d\psi$. The differential operator Δ^* is given by

$$\Delta^* = \frac{\partial^2}{\partial R^2} - \frac{1}{R}\frac{\partial}{\partial R} + \frac{\partial^2}{\partial Z^2}. \tag{33}$$

The Green function of the operator (33) is given as follows

$$G = \frac{\mu_0}{\pi k}\sqrt{RR'}\left(\left(1-\frac{1}{2}k^2\right)K(k) - E(k)\right), \tag{34}$$

where $E(k)$ and $K(k)$ are elliptic integrals of the first kind and $k^2 = 4RR'/((R+R')^2+Z^2)$. The boundary condition for (32) is a fixed boundary given as

$$\psi(R,Z) = c\ (constant) \quad (R,Z)\in\partial\Omega \tag{35}$$

where $\partial\Omega$ is the inner wall surface. The constant c in (35) is chosen to be 0. The partial differential equation (32) is called the Grad-Shafranov (GS) equation.

In the present modeling, the functional forms $F(\psi)$ and $P(\psi)$ are assumed based on prior knowledge and parameterized using free parameters. Then, using the data assimilation method described in the previous section, we obtain the equilibrium which is the solution of the (32) and (35), and the free parameters simultaneously.

B. PARAMETRIZATION

Several methods of parametrizing $F(\psi)$ and $P(\psi)$ in the model of the RFP plasma of the (32) are conceivable. In [15], the first work on the equilibrium reconstruction based on the GS equation, they use spline interpolation through several points which include unknown parameters. In the present parametrization, our strategy is to adopt a model which provides an appropriate current profile for the RFP with smaller number of unknown parameters compared with the polynomial models [9] or the spline interpolation model [15]. Consequently, we adopt a model which describes field-aligned current (force-free current) profile by two parameters and provides good approximation of experimental profiles [35], [37], [38]. Since the parametrized current profile is based on the MHD relaxation, we could advance the models for parametrization for detailed studies of the local effects of current profile on the RFP equilibrium. As for parametrization of the pressure, the plasma density and temperature profiles are parametrized separately, which could provide more physical insight in comparing the experimental results with reconstructed ones.

According to the model describing the field-aligned current by two parameters, $F' = dF/d\psi$ is expressed as

$$F' = \frac{B_{\phi 0}R_0}{\psi_{max}-\psi_{min}}\left(1+\frac{1}{\alpha}\right)\left(1-{\psi_{00}}^{\alpha}\right) \tag{36}$$

where ψ_{00} are defined as

$$\psi_{00} = \frac{\psi-\psi_{min}}{\psi_{max}-\psi_{min}}.$$

ψ_{min} is the minimum value of ψ, i.e., $\psi_{min} = \min_{R,Z}\psi(R,Z)$ and ψ_{max} is the value of ψ at boundary, i.e., $\psi_{max} = \psi(R,Z)$ at $(R,Z) \in \partial\Omega$. In the target plasma, ψ is generally a monotonic function and becomes maximum at the boundary. $B_{\phi 0}$ is the toroidal magnetic field at the position where ψ

takes its minimum value, that is, $B_{\phi 0} = B_\phi(R_{min}, Z_{min})$ where (R_{min}, Z_{min}) is so called the magnetic axis defined by

$$(R_{min}, Z_{min}) = \arg\min_{R,Z} \psi(R, Z). \tag{37}$$

The function F in (32) is determined by integrating F' with value of F at the boundary $F = F(\psi_{max}) = RB_\phi(R, Z)$, $(R, Z) \in \partial\Omega$. Note that $B_\phi(R, Z)$ at $(R, Z) \in \partial\Omega$ is the toroidal magnetic field at the boundary. It is given by a magnetic sensor attached to the plasma boundary in the experiment.

The pressure $P(\psi)$ is expressed by the product of the density $n(\psi(R, Z))$ and the temperature $k_B T(\psi(R, Z))$,

$$P(\psi) = n(\psi) k_B T(\psi) \tag{38}$$

where k_B is the Boltzmann constant. In the above equation, we parameterize the density n and the temperature T as follows

$$n = n_0(1 - {\psi_{00}}^\beta), \tag{39}$$
$$T = T_0(1 - {\psi_{00}}^\gamma) \tag{40}$$

where n_0 and T_0 are the density and temperature on the magnetic axis, respectively. The separate parametrization of the density and temperature could make it easier to distinguish their effects on the equilibrium profile, which is an advantage of the proposed method over the methods used in previous works [9], [15].

The right hands side of (32) is determined. Note that the point $(R, Z) = (R_{min}, Z_{min})$ in (37) satisfies following equations

$$\frac{\partial\psi}{\partial R}(R_{min}, Z_{min}) = 0, \quad \frac{\partial\psi}{\partial Z}(R_{min}, Z_{min}) = 0. \tag{41}$$

This equation corresponds to the (4) with $\boldsymbol{c}_k = \mathbf{0}$ $(k = 1)$. In the RFP, it is commonly observed that the ion temperature is almost as high as or even slightly higher than the electron temperature [39]–[41]. It is a clear evidence of non-collisional ion heating or acceleration mechanisms working in the RFP. In the present work we assume that radial profiles of ion temperature and density are equal to those of electrons. We define

$$\boldsymbol{p} = [B_{\phi 0}, \alpha, n_0, \beta, T_0, \gamma]^t \tag{42}$$

as the free parameters.

C. MATHEMATICAL MODEL OF SENSING PROCESSES

Figure 2 shows a poloidal cross section of the plasma and geometric arrangement of the sensors and sensing processes in RELAX. R and Z are the radial and axial coordinates shown in Fig. 1. In the following we describe the mathematical models (13) for those sensing processes.

Magnetic Sensor 1: By this sensor total toroidal plasma current I_ϕ is obtained. The process can be modeled by the integration of the toroidal current density J_ϕ over the poloidal cross section, i.e.,

$$m_1 = f_{m_1}(\psi) = \int_\Omega J_\phi(\psi(R, Z), R, Z) dS. \tag{43}$$

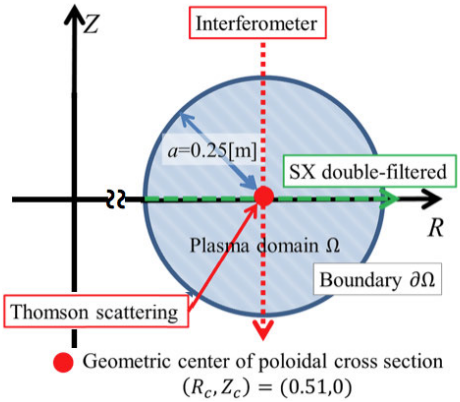

FIGURE 2. Poloidal cross section of the plasma and geometric arrangement of the sensors for plasma data in RELAX.

Magnetic Sensor 2: By this sensor the toroidal magnetic flux inside the boundary is obtained. This is modeled as

$$m_2 = f_{m_2}(\psi) = \frac{1}{\pi a^2} \int_\Omega \frac{F(\psi(R, Z))}{R} dS. \tag{44}$$

Density Sensor 1: This sensor is the interferometer which measures line-averaged electron density [42]. It is modeled as the line integral of the density in the Z direction at $R = R_c$, i.e,

$$m_3 = f_{m_3}(\psi) = (1/2a) \int_{Z_c - a}^{Z_c + a} n(R_c, Z) dZ \tag{45}$$

where (R_c, Z_c) is the geometrical center of poloidal cross section as shown in Fig. 2.

Density Sensor 2: This sensor is the Thomson scattering system which measures the electron density at the geometric center of poloidal cross section [43]. It is modeled as follows

$$m_4 = f_{m_4}(\psi) = \int_\Omega \delta(R - R_c)\delta(Z - Z_c) n(R, Z) dS. \tag{46}$$

Temperature Sensor 1: By this sensor the line averaged electron temperature is obtained based on the soft X-ray double filter method [44]. It is modeled as the line integration in the R direction at $Z = Z_c$ as follows

$$m_5 = f_{m_5}(\psi) = (1/2a) \int_{R_c - a}^{R_c + a} T(R, Z_c) dR. \tag{47}$$

Temperature Sensor 2: This sensor is the Thomson scattering system which measures the electron temperature at the geometric center of poloidal cross section [43]. It is modeled as follows

$$m_6 = f_{m_6}(\psi) = \int_\Omega \delta(R - R_c)\delta(Z - Z_c) T(R, Z) dS. \tag{48}$$

D. METHOD OF EQUILIBRIUM RECONSTRUCTION FOR RFP

In applying the proposed method in Sec. IV to the real RFP device, equations described in Sec. III are related to equations in Sec. V. The GS equation (32) with the parametrization (36), (38), (39), (40) and (42) corresponds

TABLE 1. Comparison of the reconstructed free parameter $p_{reconst}$ with their true value p_{true}.

	p_1	p_2	p_3	p_4	p_5	p_6
$\boldsymbol{p}_{true}$	4.000000	3.000000	3.000000	5.000000	4.000000	3.000000
Reconstructed ($\boldsymbol{p}_{reconst}$)	3.999918	2.999837	2.999991	4.999940	4.000132	3.000262

to the target equation (10). The boundary condition (35) corresponds to (12). The point $\boldsymbol{x}_{ex}$ satisfying (11) in Sec. III corresponds to (R_{min}, Z_{min}) satisfying (41) in Sec. V. The sensing processes from (43) to (48) ($N_m = 6$) correspond to (13). The cost function is defined by (7) where $N_m = 6$. The Algorithm for Equilibrium Reconstruction described in Sec. IV-A can be performed in the following manner for the RFP. Following the procedure for deriving the sensitivity equations described in Sec. IV, the sensitivity equations for (32) can be derived. The sensitivities $\partial\psi/\partial p_j$ are obtained by solving the GS equation (32) and its sensitivity equations thus derived. The set of $\partial m_i/\partial p_j$ is obtained by calculating (18) for $i = 1, 2, \cdots, 6$ and $j = 1, 2, \cdots, 6$ by using the sensitivities $\partial\psi/\partial p_j$ and the solution ψ, and the gradient of the cost function (7) is calculating (9). By using the gradient thus obtained, the free parameter $\boldsymbol{p}$ is updated according to an appropriate gradient based optimization method.

E. PERFORMANCE EVALUATION BY NUMERICAL EXPERIMENT

In order to evaluate the performance of the proposed method, we perform the numerical experiment, which is carried out as follows. We apply the proposed method to artificial data $m_1, m_2, \cdots, m_6$. They are obtained by solving the mathematical model (32), (36), (38), (35) and (41) of the target plasma with the parameters $\boldsymbol{p}$ being given a certain value, denoted by $\boldsymbol{p}_{true}$, and by calculating the sensing processes from (43) to (48) with the solution. We set the conditions of numerical experiment as follows. In order to mimic the real plasma experiment device RELAX, assuming that the plasma is surrounded by a perfectly conducting wall with circular cross section whose minor radius $a = 0.25$ m, in boundary condition (35) we let $\psi(R, Z) = 0$ at $(R, Z) \in \partial\Omega$, and let $\partial\Omega$ be the circle at the center $(R_c, Z_c) = (0.51\text{ m}, 0\text{ m})$ with the minor radius $a = 0.25$ m, as shown in Fig. 2.

We normalize the free parameter $\boldsymbol{p}$ as follows

$$\begin{aligned}\boldsymbol{p} &= [p_1, p_2, p_3, p_4, p_5, p_6]^t \\ &= \left[\frac{B_{\phi 0}}{\widehat{B_{\phi 0}}}, \alpha, \frac{n_0}{\widehat{n_0}}, \beta, \frac{T_0}{\widehat{T_0}}, \gamma\right]^t \end{aligned} \tag{49}$$

where $\widehat{B_{\phi 0}}$, $\widehat{n_0}$, $\widehat{T_0}$ are given as $\widehat{B_{\phi 0}} = 0.1$ T, $\widehat{n_0} = 10^{19}$ m^{-3} and $\widehat{T_0} = 10^6$ K, respectively. In the present numerical experiment, the artificial data $m_1, m_2, \cdots, m_6$ are obtained by giving the value of $\boldsymbol{p}_{true}$ as $[4, 3, 3, 5, 4, 3]^t$.

We apply the reconstruction algorithm with starting from some different initial guesses. The weights w_i of cost function (7) are chosen as $(w_1, w_2, w_3, w_4, w_5, w_6) = (1/d_1^2, 1/d_2^2, 1/d_3^2, 1/d_4^2, 1/d_5^2, 1/d_6^2)$ in order to normalize the contribution from each sensor to the cost function.

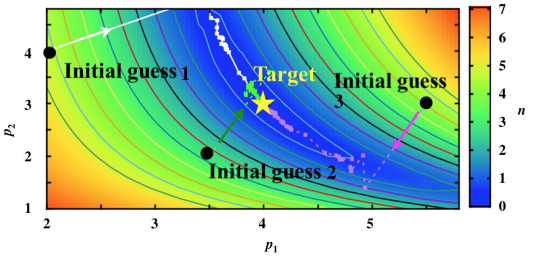

FIGURE 3. Convergence behavior of the free parameters $p_1 = B_{\phi 0}$ (normalized) and $p_2 = \alpha$ in which the trajectories in the parameter space $(p_1, p_2, \cdots, p_6)$ three initial guesses are projected onto the plane $(p_1, p_2, 3, 5, 4, 3)$.

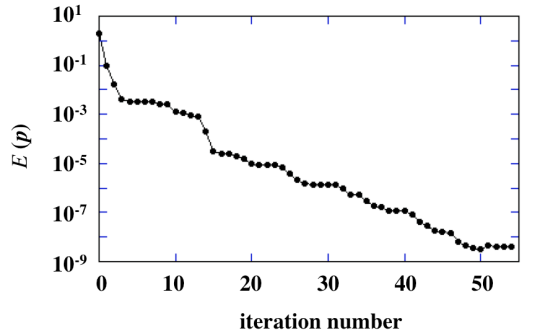

FIGURE 4. Convergence behavior of the cost function $E(\boldsymbol{p})$ versus iteration number. It corresponds to the case of initial guess 1 in Fig. 3.

Figure 3 shows typical three examples of convergence behavior of the proposed method, in which the trajectories in the parameter space $(p_1, p_2, \cdots, p_6)$ starting from three initial guesses are projected onto the plane $(p_1, p_2, 3, 5, 4, 3)$. We use the conjugate gradient method. In the figure, the values of the cost function $E(\boldsymbol{p})$ are shown in color and they are calculated on that projected plane. Color bar shows the index value n defined by $n = 10\sqrt{E}$. Note the contour lines in the figure are drawn at each 0.5 of n. The symbol ★ indicates the target optimum position $\boldsymbol{p}_{true}$ on (p_1, p_2) plane. It is seen from the figure that at each step, the free parameters are updated properly and converged to its true value $\boldsymbol{p}_{true}$ denoted by the star symbol. Figure 4 shows the convergence behavior of $E(\boldsymbol{p})$, in which horizontal axis is the number of iterations and vertical axis is the value of $E(\boldsymbol{p})$ in the case of initial guess 1 in Fig. 3. It is found that the value of $E(\boldsymbol{p})$ decreases rapidly and settles down to less than 10^{-8} after 50 iterations. In Table 1, we compare $\boldsymbol{p}_{true}$ and reconstructed value of $\boldsymbol{p}$, denoted by $\boldsymbol{p}_{reconst}$, obtained by proposed algorithm. Table 2 shows the values of the measurement data $m_1, m_2, \cdots, m_6$ calculated by using $\boldsymbol{p}_{true}$ and the reconstructed measurement data, which are calculated by using $\boldsymbol{p}_{reconst}$. For reference, the relative errors in the reconstructed measurement data are also shown. From this table, it is found that the relative errors are all in the order of 10^{-2} or less.

TABLE 2. Comparison of the obtained reconstruction data with their true value.

	plasma current m_1[kA]	average toroidal field m_2[T]	line-averaged electron density $m_3[\mathrm{m}^{-3}]$	central electron density $m_4[\mathrm{m}^{-3}]$	line-of-sight electron temperature m_5[eV]	central electron temperature m_6[eV]
$\boldsymbol{m}_{true}$	1.744698×10^{2}	7.744223×10^{-2}	2.525837×10^{19}	3.000000×10^{19}	2.611193×10^{2}	3.446888×10^{2}
Reconstructed ($\boldsymbol{m}_{reconst}$)	1.744643×10^{2}	7.743771×10^{-2}	2.525820×10^{19}	2.999991×10^{19}	2.611318×10^{2}	3.447002×10^{2}
Error[%]	-3.1567×10^{-3}	-58371×10^{-3}	-6.7018×10^{-4}	-3.0200×10^{-4}	4.7936×10^{-3}	3.3063×10^{-3}

TABLE 3. Comparison of the obtained reconstruction data with experimental data.

	measurement data (experimental and reconstructed)						
	plasma current m_1[kA]	average toroidal field m_2[T]	line-averaged electron density $m_3[\mathrm{m}^{-3}]$	central electron density $m_4[\mathrm{m}^{-3}]$	line-of-sight electron temperature m_5[eV]	central electron temperature m_6[eV]	toridal field reversal parameter (TFRP)
Shot1 (20151207020)	60.3	1.67×10^{-2}		8.13×10^{18}	46.6	76.1	-0.891
Reconstructed	60.2	1.67×10^{-2}	5.37×10^{18}	8.13×10^{18}	46.6	76.1	-0.872
Relative Error[%]	0.25	0.21		4.01×10^{-3}	4.7×10^{-2}	4.2×10^{-2}	2.1
Shot2 (20170731007)	47.4	1.54×10^{-2}	5.02×10^{18}		37.31	49.64	-0.902
Reconstructed	47.4	1.54×10^{-2}	5.01×10^{18}	7.15×10^{18}	37.14	49.81	-0.885
Relative Error[%]	0.13	0.14	6.3×10^{-2}		0.35	0.46	1.9

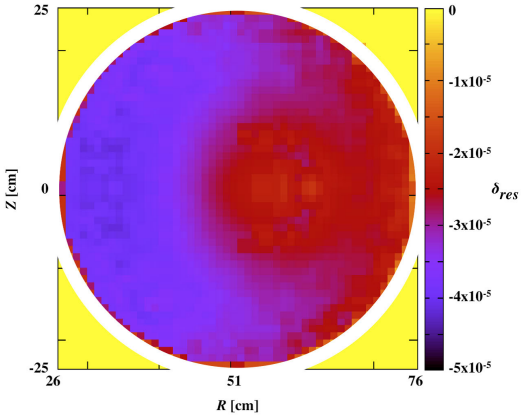

FIGURE 5. $R-Z$ distribution of residual error between target ψ_{true} and reconstructed $\psi_{reconst}$.

In order to confirm the validity of the reconstruction, we calculate the internal structure of error distribution of reconstructed ψ denoted by $\psi_{reconst}$ obtained by the proposed method. Figure 5 shows an example of two dimensional distribution in the $R-Z$ plane of the residual error between the target ψ denoted by ψ_{true} and the reconstructed $\psi_{reconst}$; the residual error is defined by $\delta_{res} = (\psi_{reconst} - \psi_{true})/\psi_{true}$. It is found from the figure that the value of the error on each mesh is in the order of 10^{-5} and internal structure is well reconstructed by the proposed method. From the results described above it can be concluded that the proposed method properly works.

F. PERFORMANCE EVALUATION BY REAL EXPERIMENT

We apply the proposed method to the data from the RFP experimental apparatus RELAX developed at Kyoto Institute of Technology. In real experiments on RELAX, a pulsed RFP discharge with a duration of ∼3 ms is produced using capacitor bank power supplies. In each discharge, a steady state during which the plasma is regarded in equilibrium is sustained for ∼2/3 of the discharge duration. A pulsed high-power laser is injected into the plasma discharge at a preset time when the central electron temperature data is obtained. An equilibrium data set at this preset time, obtained from a single discharge, is referred to as a shot and characterized by a specific number assigned to identify the discharge conditions.

Since we have no shot for which both the line-averaged density and central density are available in the data sets for the discharges with sufficient number of measurements, we have chosen those two shots as shown in Table 3: Shot 1 with the central density data but without the line averaged density data, and Shot 2, vice versa. In the experiment or analyses we set the weights w_i as $(w_1, w_2, w_3, w_4, w_5, w_6) = (1/d_1^2, 1/d_2^2, 1/d_3^2, 1/d_4^2, 1/d_5^2, 1/d_6^2)$. Optimization experiments were carried out by changing several times the initial guess of the free parameters appropriately. It is confirmed that in all the experiments the free parameters converge to the same location in the parameter space. Examples of convergence behavior of $E(\boldsymbol{p})$ in these two cases are as follows; after about 200 iterations, $E(\boldsymbol{p})$ converges and settles down to 1.1×10^{-5} for Shot 1 and to 3.7×10^{-5} for Shot 2, respectively. Table 3 shows the experimental data $(m_1, m_2, \cdots, m_6)$ from RELAX RFP machine, reconstructed data by the proposed method and their relative errors for the two shots. From this table, it is found that the relative errors are all in the order of 10^{-2} or less. Accuracy of the reconstructed equilibria is acceptable because the errors are smaller than uncertainties in the experimental data in a single shot, ranging from ∼1 % to ∼10 % depending upon the diagnostics or sensors.

Table 3 also shows the values of the toroidal field reversal parameter (TFRP) defined by the ratio of the edge toroidal field to the cross-sectional averaged toroidal field, and characterizes the approximate equilibrium properties near the plasma edge. The value of TFRP is around -0.9 in these two shots, indicating that the magnetic field profiles near the edge are similar to each other for these shots, and therefore, we will concentrate on the core properties in evaluating the reconstructed results. Based on these facts, we study the

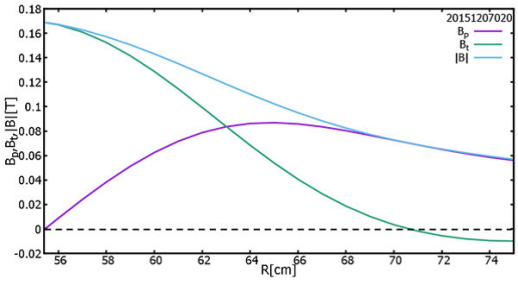

FIGURE 6. Radial profiles of the reconstructed toroidal and poloidal magnetic field.

validity of the reconstructed equilibrium. Figure 6 shows the toroidal and poloidal magnetic field profiles calculated from the reconstructed poloidal flux function $\psi_{reconst}$ for the case of Shot 1 in Table 3. The horizontal axis starts from the location of the magnetic axis which is shifted outward by ∼5 cm from the geometrical center of the wall surrounding the plasma. This outward shift is known to be brought about by the plasma pressure effect [22]. The toroidal magnetic field indicated by the green line reverses around $R = 71$ cm, which shows production of typical RFP plasma.

In real experiment, it is impossible to evaluate the reconstructed magnetic field profiles by comparing them with their real profiles. Therefore, the safety factor profile is calculated from the reconstructed magnetic field profiles. Since the MHD behavior of the plasma is sensitive to the safety factor profile, we compare the MHD behavior in the experiment with the reconstructed safety factor profile to evaluate the validity of the reconstruction.

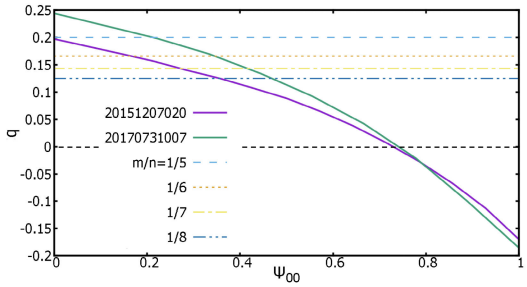

FIGURE 7. Radial profiles of the safety factor calculated from the reconstructed magnetic field.

From the internal magnetic field profiles, the safety factor $q = <(rB_\phi)/(RB_p)>$ can be plotted as shown in Fig. 7, where $<\cdots>$ denotes the average over the flux surface. Here, the safety factor is the ratio of the average number of toroidal circulation to one poloidal circulation of the magnetic field lines. In MHD equilibrium, magnetic field lines lie on nested closed surfaces known as magnetic surfaces. The safety factor is therefore a surface quantity and a measure of twistedness of magnetic field line, which characterizes the equilibrium. On a mode rational surface where $q = m/n$ (m and n are the integers), the magnetic field line closes after n turns in poloidal and m turns in toroidal direction. Some classes of MHD instabilities tend to grow when the wave number vector becomes perpendicular to the magnetic field line on the mode rational surface.

Next, by comparing the position of the mode rational surface predicted from the reconstructed distribution of the safety factor with the wavenumber spectrum of the magnetic field fluctuation power measured in the edge plasma, the consistency between them is examined. The wavenumber is known to be closely related to the profile of the safety factor. It is not input experimental data for reconstruction. Therefore, the wavenumber can be used as a measure for consistency of the reconstructed magnetic field profile.

Figure 7 shows the radial profile of the safety factor q for the normalized poloidal magnetic flux calculated from the magnetic field distribution and is the result of "Shot 1" in Table 3. The safety factor on the magnetic axis $q(0)$ is about 0.2 to 0.25, and the mode rational surface closest to the magnetic axis is $q = 1/5$. In RFP experiments and nonlinear MHD simulation studies so far, it has been shown that in the RFP configuration, MHD instability with a resonance surface inside the plasma grows and nonlinearly saturates, its amplitude reaching a (quasi) steady state. It is known that the amplitude of the instability having the resonant surface close to the magnetic axis is the largest and amplitudes decrease for higher modes. In RELAX, the properties of magnetic field fluctuation in the discharge region of the plasma ($-0.8 <$ TFRP < -0.6) have been studied in detail [45], discharge region of which is almost the same as the RFP targeted for the present equilibrium reconstruction. We should note again that toroidal field reversal parameter is usually denoted by "F", however, we use TFRP instead, in order to avoid confusion with the poloidal current function F in GS equation. The mode number of fluctuation where it is maximized (instability saturated nonlinearly) is $m = 1$, $n = 5$. This suggests that the mode rational surface close to the magnetic axis is $q = 1/5$, which is consistent with the distributions of the safety factor (Fig. 7) obtained from the reconstructed poloidal flux. From the above, the equilibrium obtained by the proposed method is proved to be reasonable. Therefore it can be concluded that the proposed method properly works for real experimental data.

G. REMARKS ON EXPERIMENTAL RESULTS

The pressure and the current density profiles are properly reconstructed with the proposed method. It is also possible to evaluate the stability margin of the plasma from the results of reconstruction. One of the important figures of merit for fusion plasma is the normalized pressure, the ratio of the plasma kinetic pressure (density × temperature) to the pressure of the magnetic field for plasma confinement. The proposed method for equilibrium reconstruction could play an important role in achieving high performance plasmas, by providing appropriate targets for precise plasma control. In the present equilibrium reconstruction of the real RFP experiment, it is found that normalized plasma pressure is estimated approximately to be 1.72% for the case of Shot 1,

which suggests that both the density and the temperature must be improved in achieving high performance RFP plasma. In order to achieve higher density, fuel particles must be introduced while controlling the wall conditions. In order to achieve higher temperature, in addition to improving the plasma confinement, higher Ohmic heating power is necessary while keeping the current density profile to be stable to MHD instabilities.

VI. CONCLUSION

Determination of the magnetohydrodynamic (MHD) equilibrium is of fundamental importance in the study of equilibrium related issues in magnetic fusion plasmas. In this paper, we propose a method of reconstructing equilibrium of magnetic fusion plasma based on data assimilation. Aiming to apply not only to axisymmetric plasmas but also to plasmas which do not have toroidal symmetry, we formulate the problems of equilibrium reconstruction in generalized forms and derive methods to solve them. We also propose a method for applying it to the reversed field pinch (RFP) plasma.

The validity and performance of the proposed method are demonstrated through numerical experiments and also real experiments using RELAX device developed at Kyoto Institute of Technology. It is shown through numerical experiments that the proposed method possesses enough accuracy and convergence, and through real experiments that the reconstructed profile is consistent with observed MHD phenomena of the target plasma. It is therefore concluded that the equilibrium of plasma can be appropriately reconstructed by the proposed method, which could play important roles in the study of equilibrium of fusion plasmas.

For future works the followings are considered. In the proposed method, the optimization is performed by deriving the sensitivity equations in which computation time increases in proportion to the number of unknown parameters. In order to solve this problem it is considered to utilize the optimization by deriving the adjoint equations, which is under progress. Furthermore, in the present proposed method, we formulate the equilibrium reconstruction problems in generalized forms and derive methods to solve them, aiming to apply it to plasmas without toroidal symmetry. In axisymmetric toroidal plasmas such as tokamak and RFP, helically deformed equilibrium states have attracted much attention in the last decades because of the following reasons. In the RFP, the equilibrium with helical magnetic axis has a potential of confinement with perfect magnetic surfaces [46]–[48]. In the tokamak, the equilibrium with helically deformed hot core was first recognized as the snake, and such configurations are expected to play important roles in the advanced tokamak operation scenarios [49]. Extension of application of the proposed method to the reconstruction problem of general toroidal plasmas is one of the future works.

ACKNOWLEDGMENT

The authors thank Dr. R. Paccagnella of Consorzio RFX for fruitful discussion. They also thank Prof. T. Mine and Prof. H. Himura of Kyoto Institute of Technology for their supports. Akio Sanpei thanks Prof. A. Ejiri and Prof. N. Tsujii of the University of Tokyo for valuable comments about reconstruction technique.

REFERENCES

[1] D. J. Ward, N. P. Taylor, and I. Cook, "Economically acceptable fusion power stations with safety and environmental advantages," *Fusion Eng. Des.*, vols. 58–59, pp. 1033–1036, Nov. 2001.
[2] W. Manheimer, "Mid century carbon free sustainable energy development based on fusion breeding," *IEEE Access*, vol. 6, pp. 64954–64969, Oct. 2018.
[3] B. Bigot, "Progress toward ITER's first plasma," *Nucl. Fusion*, vol. 59, no. 11, Jun. 2019, Art. no. 112001.
[4] L. Marrelli, R. Cavazzana, D. Bonfiglio, and M. Gobbin, "Upgrades of the RFX-mod reversed field pinch and expected scenario improvements," *Nucl. Fusion*, vol. 59, no. 7, Jun. 2019, Art. no. 076027.
[5] W. Capecchi, J. K. Anderson, P. J. Bonofiglo, J. Kim, R. M. Magee, K. J. McCollam, R. McConnell, E. Parke, and J. S. Sarff, "A measure of fast ion beta at marginal stability in the reversed field pinch," *Nucl. Fusion*, vol. 59, no. 8, Jun. 2019, Art. no. 086026.
[6] A. C. Setiadi, P. R. Brunsell, and L. Frassinetti, "Improved model predictive control of resistive wall modes by error field estimator in EXTRAP T2R," *Plasma Phys. Controlled Fusion*, vol. 58, no. 12, Sep. 2016, Art. no. 124002.
[7] W. Liu, T. Lan, W. Mao, H. Li, J. Xie, A. Liu, and S. Wan, "Overview of keda torus eXperiment initial results," *Nucl. Fusion*, vol. 57, no. 11, Aug. 2017, Art. no. 116038.
[8] S. Masamune A. Sanpei, Y. Aoki, T. Nagano, M. Higuchi, R. Tsuboi, S. Nakanobo, H. Himura, N. Mizuguchi, T. Akiyama, T. Mizuuchi, K. J. McCollam, D. J. Den Hartog, and R. Paccagnella, "Improved low-aspect-ratio RFP performance with active MHD control and associated change in magnetic topology in RELAX," in *Proc. IAEA Fusion Energy Conf.*, 2016, pp. 1–4.
[9] L. L. Lao, H. St. John, R. D. Stambaugh, A. G. Kellman, and W. Pfeiffer, "Reconstruction of current profile parameters and plasma shapes in Tokamaks," *Nucl. Fusion*, vol. 25, no. 11, pp. 1611–1622, Nov. 1985.
[10] J. R. Ferron, M. L. Walker, L. L. Lao, H. E. S. John, D. A. Humphreys, and J. A. Leuer, "Real time equilibrium reconstruction for Tokamak discharge control," *Nucl. Fusion*, vol. 38, no. 7, pp. 1055–1066, Jul. 1998.
[11] J.-M. Moret, B. P. Duval, H. B. Le, S. Coda, F. Felici, and H. Reimerdes, "Tokamak equilibrium reconstruction code LIUQE and its real time implementation," *Fusion Eng. Des.*, vol. 91, pp. 1–15, Feb. 2015.
[12] B. S. Yuan, X. Q. Ji, Y. G. Li, Y. Xu, Y. Zhou, L. M. Yu, S. Y. Liang, and T. F. Sun, "Study of plasma equilibrium reconstruction on HL-2A," *Fusion Eng. Des.*, vol. 134, pp. 5–10, Sep. 2018.
[13] P. J. McCarthy, P. Martin, and W. Schneider, "The CLISTE interpretive equilibrium code," IPP, Müchen, Germany, Tech. Rep. 5/85, May 1999.
[14] J. Blum, C. Boulbe, and B. Faugeras, "Reconstruction of the equilibrium of the plasma in a Tokamak and identification of the current density profile in real time," *J. Comput. Phys.*, vol. 231, no. 3, pp. 960–980, Feb. 2012.
[15] J. K. Anderson, C. B. Forest, T. M. Biewer, J. S. Sarff, and J. C. Wright, "Equilibrium reconstruction in the madison symmetric torus reversed field pinch," *Nucl. Fusion*, vol. 44, no. 1, pp. 162–171, Jan. 2004.
[16] L. Bengtsson, *Dynamic Meteorology: Data Assimilation Methods* (Applied Mathematical Sciences). New York, NY, USA: Springer-Verlag, 1981.
[17] M. Sharan, *Data Assimilation and Its Applications*. Basel, Switzerland: Springer, 2012.
[18] M. Asch, *Data Assimilation: Methods, Algorithms, and Applications*. Philadelphia, PA, USA: Society for Industrial and Applied Mathematics, 2016.
[19] Z. H. Ismail and N. A. Jalaludin, "Robust data assimilation in river flow and stage estimation based on multiple imputation particle filter," *IEEE Access*, vol. 7, pp. 159226–159238, Oct. 2019.
[20] M. Eltahan and S. Alahmadi, "Numerical dust storm simulation using modified geographical domain and data assimilation: 3DVAR and 4DVAR (WRF-Chem/WRFDA)," *IEEE Access*, vol. 7, pp. 128980–128989, Jul. 2019.
[21] H. Grad and H. Rubin, "Hydromagnetic equilibria and force-free fields," in *Proc. 2nd UN Conf. Peaceful Uses At. Energy*, vol. 31, 1958, pp. 190–197.
[22] V. D. Shafranov, "Equilibrium of a toroidal pinch in a magnetic field," *At. Energy*, vol. 13, no. 6, pp. 521–529, Dec. 1962.

[23] M. Wakatani, *Stellarator and Heliotron Devices*. New York, NY, USA: Oxford Univ. Press, 1988.
[24] S. Masamune, A. Sanpei, R. Ikezoe, T. Onchi, K. Murata, K. Oki, H. Shimazu, T. Yamashita, and H. Himura, "Characterization of initial low-aspect ratio RFP plasmas in 'RELAX,'" *J. Phys. Soc. Jpn.*, vol. 76, no. 12, Nov. 2007, Art. no. 123501.
[25] V. D. Pustovitov, "Magnetic diagnostics: General principles and the problem of reconstruction of plasma current and pressure profiles in toroidal systems," *Nucl. Fusion*, vol. 41, p. 721, Jun. 2001.
[26] H. Anand, C. Galperti, S. Coda, B. P. Duval, F. Felici, T. Blanken, E. Maljaars, J.-M. Moret, O. Sauter, T. P. Goodman, and D. Kim, "Distributed digital real-time control system for the TCV Tokamak and its applications," *Nucl. Fusion*, vol. 57, no. 5, May 2017, Art. no. 056005.
[27] F. Carpanese, F. Felici, C. Galperti, A. Merle, J. M. Moret, O. Sauter, and TCV, "First demonstration of real-time kinetic equilibrium reconstruction on TCV by coupling LIUQE and RAPTOR," *Nucl. Fusion*, vol. 60, no. 6, Jun. 2020, Art. no. 066020.
[28] E. Picard, *Traité d'analyse Tome II*. Paris, France: Gauthier-Villars, 1893.
[29] J. B. Taylor, "Relaxation of toroidal plasma and generation of reverse magnetic fields," *Phys. Rev. Lett.*, vol. 33, p. 1139, Jun. 1974.
[30] W. Shen and J. C. Sprott, "Modified polynomial function model for reversed-field pinches," *Phys. Fluids B: Plasma Phys.*, vol. 3, p. 1225, Jan. 1991.
[31] J. S. Sarff, S. A. Hokin, H. Ji, S. C. Prager, and C. R. Sovinec, "Fluctuation and transport reduction in a reversed field pinch by inductive poloidal current drive," *Phys. Rev. Lett.*, vol. 72, p. 3670, Jun. 1994.
[32] P. Martin, A. Buffa, S. Cappello, and F. D'Angelo, "Quasi-single helicity states in the reversed field pinch: Beyond the standard paradigm," *Phys. Plasmas*, vol. 7, p. 1984, May 2000.
[33] D. F. Escande, P. Martin, S. Ortolani, A. Buffa, and P. Franz, "Quasi-single-helicity reversed-field-pinch plasmas," *Phys. Rev. Lett.*, vol. 85, p. 1662, Aug. 2000.
[34] L. Marrelli, P. Martin, M. E. Puiatti, J. S. Sarff, B. E. Chapman, J. R. Drake, D. F. Escande, and S. Masamune, "The reversed field pinch," *Nucl. Fusion*, vol. 61, Jan. 2021, Art. no. 023001.
[35] S. Ortolani and D. D. Schnack, *Magnetohydrodynamics of Plasma Relaxation*. Singapore: World Scientic, 1993.
[36] J. A. Nelder and R. Mead, "A simplex method for function minimization," *Comput. J.*, vol. 7, no. 4, pp. 308–313, Jan. 1965.
[37] V. Antoni, D. Merlin, S. Ortolani, and R. Paccagnella, "MHD stability analysis of force-free reversed field pinch configurations," *Nucl. Fusion*, vol. 26, no. 12, pp. 1711–1788, Dec. 1986.
[38] R. Paccagnella, A. Bondeson, and H. Lütjens, "Ideal toroidal stability beta limits and shaping effects for reversed field pinch configurations," *Nucl. fusion*, vol. 31, no. 10, pp. 1899–1908, Oct. 1991.
[39] M. Zuin, W. Schneider, and A. Barzon, "Ion temperature measurements by means of a neutral particle analyzer in RFX-mod plasmas," in *Proc. 38th EPS Conf. Plasma Phys.*, Strasbourg, France, Jun./Jul. 2011 p. 2.
[40] E. Scime, M. Cekic, D. J. Den Hartog, and S. Hokin, "Ion heating and magnetohydrodynamic dynamo fluctuations in the reversed-field pinch," *Phys. Plasmas*, vol. 4, p. 4062, Aug. 1992.
[41] R. Gatto and P. W. Terry, "Anomalous ion heating from ambipolar-constrained magnetic fluctuation-induced transport," *Phys. Plasmas*, vol. 8, p. 825, Feb. 2001.
[42] M. Sugihara, K. Oki, R. Ikezoe, T. Onchi, A. Sanpei, H. Himura, S. Masamune, T. Akiyama, A. Ejiri, K. Sakamoto, K. Nagasaki, and V. Zhuravlev, "Density regimes of low-aspect-ratio RFP plasmas in RELAX," *Plasma Fusion Res.*, vol. 5, p. S2061, Dec. 2010.
[43] R. Ueba, S. Masamune, A. Sanpei, K. Uchiyama, H. Tanaka, K. Nishimura, G. Ishi, R. Kodera, H. Himura, D. J. Den Hartog, and H. Koguchi, "Electron temperature measurement by Thomson scattering in a low-aspect-ratio RFP RELAX," *Plasma Fusion Res.*, vol. 9, Feb. 2014, Art. no. 1302009.
[44] K. Nishimura, A. Sanpei, H. Tanaka, G. Ishii, R. Kodera, R. Ueba, H. Himura, S. Masamune, S. Ohdachi, and N. Mizuguchi, "2D electron temperature diagnostic using soft X-ray imaging technique," *Rev. Sci. Instrum.*, vol. 85, no. 3, Mar. 2014, Art. no. 033502.
[45] R. Ikezoe, K. Oki, T. Onchi, Y. Konishi, M. Sugihara, S. Fujita, A. Sanpei, H. Himura, and S. Masamune, "Extended operational regimes and MHD behavior in a low-aspect-ratio reversed field pinch in RELAX," *Plasma Phys. Controlled Fusion*, vol. 53, no. 2, Feb. 2011, Art. no. 025003.
[46] E. Martines, R. Lorenzini, B. Momo, D. Terranova, P. Zanca, A. Alfier, F. Bonomo, A. Canton, A. Fassina, P. Franz, and P. Innocente, "Equilibrium reconstruction for single helical axis reversed field pinch plasmas," *Plasma Phys. Controlled Fusion*, vol. 53, no. 3, Feb. 2011, Art. no. 035015.
[47] D. Terranova, M. Gobbin, and A. H. Boozer, "Self-organized helical equilibria in the RFX-mod reversed field pinch," *Contrib. Plasma Phys.*, vol. 50, no. 8, p. 775, Jul. 2010.
[48] J. D. Hanson, S. P. Hirshman, S. F. Knowlton, L. L. Lao, E. A. Lazarus, and J. M. Shields, "V3FIT: A code for three-dimensional equilibrium reconstruction," *Nucl. Fusion*, vol. 49, no. 7, Jul. 2009, Art. no. 075031.
[49] W. A. Cooper, I. T. Chapman, and O. Schmitz, "Bifurcated helical core equilibrium states in tokamaks," *Nucl. Fusion*, vol. 53, Jun. 2013, Art. no. 073021.

AKIO SANPEI (Member, IEEE) received the B.Sc., master's, and Ph.D. degrees from Kyoto University, Kyoto, Japan, in 1999, 2001, and 2004, respectively.

In 2004, he joined the Department of Electronics, Kyoto Institute of Technology, Kyoto, as an Assistant Professor, where he became a Lecturer, in 2014, and has been an Associate Professor, since 2019. His current research interests include plasma science, dusty plasmas, fusion plasma, and nonneutral plasma.

TAKAYUKI OKAMOTO received the B.S. and M.S. degrees from the Kyoto Institute of Technology, Kyoto, Japan, in 2017 and 2019, respectively. He is currently working with IDEC Corporation.

SADAO MASAMUNE received the B.Eng., M.Eng., and Ph.D. degrees in nuclear engineering from Kyoto University, Kyoto, Japan, in 1976, 1978, and 1984, respectively.

In 1982, he joined the Kyoto Institute of Technology (KIT), Kyoto, as an Assistant Professor, and was promoted to an Associate Professor, in 1988. He was a Visiting Scientist with the Los Alamos National Laboratory, from 1985 to 1986 and in 1989. He was a Visiting Scientist with Kernfroshungsanlage Jülich, in 1987. He was a Visiting Faculty Member with the University of Wisconsin-Madison, in 1996. From 2000 to 2019, he was a Full Professor with KIT. He was a Visiting Professor with the National Institute for Fusion Science (NIFS), from 2010 to 2011. He was a Visiting Professor with the Institute of Advanced Energy, Kyoto University, in 2012. In 2019, he joined the College of Engineering, Chubu University, Kasugai, Japan, as a Full Professor. His research interest includes fusion plasma science, with emphasis on MHD phenomena associated with relaxation or self-organization in fusion plasmas.

YASUAKI KUROE (Life Member, IEEE) received the B.S. and M.S. degrees in instrumentation engineering and the Ph.D. degree in industrial science from Kobe University, Kobe, Japan, in 1974, 1977, and 1982, respectively. In 1982, he joined the Department of Electrical Engineering, Kobe University, as an Assistant Professor. In 1991, he moved to the Department of Electronics and Information Science, Kyoto Institute of Technology, Kyoto, Japan, as an Associate Professor, and became a Professor. Since 2016, he has been a Professor Emeritus with the Kyoto Institute of Technology. He is currently a Visiting Professor with the Faculty of Engineering Science, Kansai University, Osaka, Japan, and a Research Fellow with Doshisha University, Kyoto. His current research interests include computational intelligence, control and system theory and its applications, and computer aided analysis and design.